Laponite-stabilized iron oxide nanoparticles for in vivo MR imaging of tumors

Journal:	*Biomaterials Science*
Manuscript ID	BM-ART-11-2015-000508.R1
Article Type:	Paper
Date Submitted by the Author:	10-Dec-2015

Complete List of Authors:	Ding, Ling; Donghua University, College of Chemistry, Chemical Engineering, and Biotechnology Hu, Yong; Donghua University, College of Chemistry, Chemical Engineering, and Biotechnology Luo, Yu; Donghua University, College of Chemistry, Chemical Engineering, and Biotechnology Zhu, Jianzhi; Donghua University, College of Chemistry, Chemical Engineering, and Biotechnology Wu, Yilun; Donghua University, Yu, Zhibo; Donghua University, College of Chemistry, Chemical Engineering, and Biotechnology Cao, Xueyan; Donghua University, Peng, Chen; Shanghai Tenth People's Hospital, School of Medicine, Tongji Univesity, Department of Radiology Shi, Xiangyang; Donghua University, College of Chemistry, Chemical Engineering, and Biotechnology Guo, Rui; Donghua University, College of Chemistry, Chemical Engineering and Biotechnology

Biomaterials Science

ARTICLE

Laponite-stabilized iron oxide nanoparticles for *in vivo* MR imaging of tumors

Received 00th xx 20xx,
Accepted 00th xx 20xx

DOI: 10.1039/x0xx00000x

www.rsc.org/

Ling Ding,[‡a] Yong Hu,[‡a] Yu Luo,[a] Jianzhi Zhu,[a] Yilun Wu,[a] Zhibo Yu,[a] Xueyan Cao,[a] Chen Peng,*[b] Xiangyang Shi,*[ac] Rui Guo*[a]

We report the synthesis, characterization and utilization of laponite stabilzed magnetic iron oxide nanoparticles (LAP-Fe_3O_4 NPs) as a high performance contrast agent for *in vivo* magnetic resonance (MR) detection of tumors. In this study, Fe_3O_4 NPs were synthesized by a facile controlled coprecipitation route in LAP solution, and the formed LAP-Fe_3O_4 NPs have great colloidal stability and about 2-fold increase of T_2 relaxivity than Fe_3O_4 NPs (from 247.6 $mM^{-1}s^{-1}$ to 475.9 $mM^{-1}s^{-1}$). Moreover, cytotoxicity assay and cell morphology observation demonstrate that LAP-Fe_3O_4 NPs display good biocompatibility in the given Fe concentration range, and *in vivo* biodistribution results prove that NPs can be metabolized and cleared out of body. Most importantly, LAP-Fe_3O_4 NPs can not only be used as a contrast agent for MR imaging of cancer cells *in vitro* due to the effective uptake by tumor cells, but also significantly enhance the contrast of a xenografted tumor model. Therefore, the developed LAP-based Fe_3O_4 NPs with good colloidal stability and exceptionally high transverse relaxivity may have tremendous potential in MR imaging applications.

Introduction

Magnetic resonance (MR) imaging is an indispensable medical diagnostic technique that has been frequently used to obtain real time 3D images of body tissues based on the difference in ^1H NMR signal of water in different tissues. Compared to other imaging techniques, MR imaging is able to produce images with good spatial and temporal resolution, excellent soft tissue contrast, and deep tissue penetration without the need of ionizing radiation. However, MR imaging does have its disadvantages and the major one is represented by its limited sensitivity. In order to enhance the contrast between normal tissues and pathological areas, MR imaging contrast agents are often used to help differentiate cells and tissues that are magnetically similar but histologically distinct.[1-6]

Superparamagnetic iron oxides nanoparticles (Fe_3O_4 NPs) are a type of important MR imaging contrast agents which were received considerable interest because of their high saturation magnetization and low toxicity. The high T_2 relaxivity of Fe_3O_4 NPs results in faster spin-spin relaxation of protons in their vicinity and hence darkens T_2-weighted MR images.[2, 7-9] Tissues that have phagocytic function or leaky vasculature will enrich the Fe_3O_4 NPs and show lower signal in T_2-weighted image, whereas pathological tissues lacking functional phagocytes will stand out in the image. However, Fe_3O_4 NPs have a high tendency toward aggregation due to their large surface area and strong magnetic property. As a result, different stabilizers, such as chitosan,[7] polyethyleneimine (PEI),[10, 11] dendrimer,[12-15] peptide,[16] neurotransmitter[17] and inorganic silica[18] have been applied to provide required colloidal stability for Fe_3O_4 NPs as contrast agents. Unfortunately, the use of those stabilizers typically causes a considerable decline in T_2 relaxivity and reduces MR imaging contrast enhancement compared to the naked Fe_3O_4 NPs,[19, 20] meaning that more contrast agents have to be administrated for satisfactory imaging and may enhance the potential for harmful side effects. Therefore, it is highly desirable and a great challenge to synthesize Fe_3O_4 NPs-based MR imaging contrast agent with improved T_2 relaxivity, good colloidal stability and biocompatibility.

Laponite (LAP) is a kind of synthetic nanoclay smectite and has a typical layered structure similar to natural hectorite. LAP can be stably dispersed in water as individual nanodisks with a diameter of 25 nm and a thickness of 1 nm, having negative change on the surface and slight positive charge on the edge.[21, 22] The high specific surface area along with the unique charge distribution characteristics has led to many interesting mutual interaction behaviors between LAP nanodisks and other molecules, and hence LAP has been used in personal care, surface coatings, paper treatment and

[a] College of Chemistry, Chemical Engineering and Biotechnology, Donghua University, Shanghai 201620, People's Republic of China. E-mail: ruiguo@dhu.edu.cn; xshi@dhu.edu.cn
[b] Department of Radiology, Shanghai Tenth People's Hospital, School of Medicine, Tongji University, Shanghai, 200072, People's Republic of China. E-mail: cpengrr@gmail.com
[c] State Key Laboratory for Modification of Chemical Fibers and Polymer Materials, Donghua University, Shanghai, 201620, People's Republic of China.
† Electronic Supplementary Information (ESI) available: additional experimental results. See DOI: 10.1039/x0xx00000x
‡ These authors equally contributed to this work.

other fields.[23-25] Due to its good biocompatibility and inertness, LAP's potential applications have recently been extended to biomedical fields such as drug delivery,[26-30] immobilization of DNA or proteins for biosensing,[31, 32] and synthesis of inorganic nanoparticles with biomedical functionalities.[33-35] In our previous work, anticancer drug doxorubicin (DOX) was loaded on LAP nanodisks at a high loading efficiency due to its special cation exchange capacity, and the resultant composites showed a significantly higher cancer cell inhibition efficacy than free DOX and afforded the treated mice with dramatically prolonged survival time.[26, 27] When targeting agents, such as folic acid or lactobionic acid, are conjugated on LAP's surface, the modified LAP can specifically deliver drugs to tumor cells and display targeted inhibition efficacy.[29, 30] Moreover, LAP has been demonstrated as an attractive matrix for the enzyme immobilization in the design of biosensor because of its strong adsorption property and high hydrophilicity.[36, 37] In another interesting work by Tzitzios et al.,[38] LAP/γ-Fe_2O_3 NPs were synthesized by a one step precipitation method and they reported an improved relaxivity over mono-dispersed γ-Fe_2O_3 NPs, though no *in vivo* MR imaging contrast enhancement effect of the obtained LAP/γ-Fe_2O_3 was presented.

In the present study, we utilized a facile controlled coprecipitation method to develop a novel water-dispersible LAP-Fe_3O_4 NPs (Scheme 1). The synthesized LAP-Fe_3O_4 NPs extensively characterized *via* transmission electron microscopy (TEM), X-Ray diffraction analysis (XRD), dynamic light scattering (DLS), inductively coupled plasma-optical emission spectroscopy (ICP-OES), and FTIR spectrometry. And the cytotoxicity of LAP-Fe_3O_4 NPs was assessed by cell viability assay and cell morphology observation. Finally, their MR imaging performance was evaluated *in vitro* and *in vivo* using a human cervical carcinoma cell line (HeLa cells) and the HeLa xenografted tumor model, respectively. To the best of our knowledge, this is the first study reporting on the development of LAP-Fe_3O_4 NPs as a promising negative MR imaging contrast agent for *in vivo* MR imaging of tumors.

Experimental

Materials

Laponite ($Na^{+0.7}[(Si_8Mg_{5.5}Li_{0.3})O_{20}(OH)_4]^{-0.7}$, LAP) was purchased from Zhejiang Institute of Geologic and Mineral Resources (Hangzhou, China). Ferric chloride hexahydrate ($FeCl_3{\cdot}6H_2O$ > 99%), ferrous chloride tetrahydrate ($FeCl_2{\cdot}4H_2O$ > 99%), sodium hydroxide and hydrochloric acid (HCl = 37%) were obtained from Aldrich. HeLa cells (a human cervical carcinoma cell line) were obtained from Institute of Biochemistry and Cell Biology, the Chinese Academy of Sciences (Shanghai, China). 3-(4,5-Dimethylthiazol-2-yl)-2,5-diphenyltetrazolium bromide (MTT) was supplied by Shanghai Sangon Biological Engineering Technology & Services Co., Ltd (Shanghai, China). Perls stain was from Beijing Leagene Biotechnology Co., Ltd (Beijing, China). Dulbecco's modified Eagle medium (DMEM), fetal bovine serum (FBS), penicillin, and streptomycin were purchased from Hangzhou Jinuo Biomedical Technology Co., Ltd. (Hangzhou, China). All chemicals purchased were used without further purification. Water with a resistivity of 18.2 MΩ cm was purified by a Milli-Q Plus 185 water purification system (Millipore, Bedford, MA) to be used.

Synthesis of LAP-Fe_3O_4 NPs

LAP-Fe_3O_4 NPs were prepared by a facile controlled coprecipitation approach in the presence of LAP under N_2 atmosphere.[19] In brief, 500 mg of LAP powder was dispersed into 50 mL water and vigorously stirred overnight to obtain a homogeneous suspension. The suspension was then transferred into a three-neck round-bottom flask and degassed with bubbling N_2 by magnetic stirring for 10 min at 80 °C. Then, 15 mL aqueous solution (containing 0.089 mL HCl) of $FeCl_3{\cdot}\ 6H_2O$ (0.721 g) and $FeCl_2{\cdot}4H_2O$ (0.265 g) was added into the LAP solution under N_2 bubbling. After 10 min, 10 mL of NaOH (2.0 g) aqueous solution was quickly added into the above mixture under high-speed stirring. The whole reaction was protected under N_2 atmosphere at 80 °C and was vigorously stirred for another 2 h. Then the black precipitate was magnetically separated and washed 3-5 times with water until stable ferrofluid was obtained. Thus, LAP-Fe_3O_4 NPs were successfully prepared. For comparison, Fe_3O_4 NPs were prepared without LAP under the same conditions.

Characterization

The Fe and Mg concentrations of samples were analyzed by a Leeman Prodigy ICP-OES system (Hudson, NH). TEM was carried out with a JEOL 2010 analytical electron microscope (Tokyo, Japan) operating at 200 kV to characterize the morphology and size of the NPs. Before measurements, the samples were prepared by putting a drop of diluted NP suspension (6 μL) onto a carbon-coated copper grid and dried in air. For each sample, at least 200 particles in different TEM images were randomly selected and measured by using an ImageJ software to calculate the size distribution of the NPs. Hydrodynamic size and zeta potential were measured using a Malvern Zetasizer Nano ZS model ZEN3600 (Worcestershire, UK) equipped with a standard 633 nm laser. Before measurements, the samples were dispersed in water at a NP concentration of 0.1 mg mL^{-1}. The crystalline structure of NPs was measured using XRD by step scan in the Rigaku D/max-2550 PC X-ray diffractometer (Rigaku Co., Tokyo, Japan) equipped with Cu Kα radiation (λ = 0.154 nm) at 40 kV and 200 mA. The examined 2ϑ range was from 0° to 60°. FTIR spectra were acquired using a Nicolet Nexus 670 FTIR (Nicolet-Thermo) spectrometer. The spectra of all samples were recorded by a transmission mode with wavenumber in a range of 400-4000 cm^{-1}. Before analysis, the dry samples mixed with ground KBr crystals were pressed as pellets. T_2 relaxometry was measured by a 0.5 T NMI20-Analyst NMR Analyzing and Imaging system (Niumag Corporation, Shanghai, China). The samples were diluted in water with Fe concentration in the range of 0.005-0.08 mM.

The instrumental parameters were set at point resolution of 156 mm × 156 mm, section thickness of 0.6 mm, TR of 5800 ms, TE of 100 ms, and number of excitation = 1. The T_2 relaxivity of NPs was calculated by a linear fitting of the inverse T_2 ($1/T_2$) relaxation time as a function of Fe concentration (mM).

Cell culture

HeLa cells were continuously cultured in 25-cm^2 plates with 5 mL of DMEM containing 1% penicillin-streptomycin and 10% FBS in an incubator with 5% CO_2 at 37 °C. The cells were passaged every 3 days when approaching to the density of 80%-90%.

Cytotoxicity assay and cell morphology observation

The viability of HeLa cells treated with LAP-Fe_3O_4 NPs *in vitro* was assessed by MTT assay. Briefly, 1×10^4 HeLa cells were seeded into a 96-well plate with 200 μL DMEM per well and incubated overnight at 37 °C and 5% CO_2 to bring the cells to confluence. Then the medium was replaced with 200 μL fresh medium containing PBS (control), LAP-Fe_3O_4 NPs with an Fe concentration ranging from 10 to 100 μg mL^{-1}. After 24 h incubation, MTT (20 μL in PBS, 5 mg mL^{-1}) was added to each well. After an additional 4 h incubation, 150 μL DMSO was added to replace the medium. Then the plate was gently shaken for 10 min to dissolve the insoluble formazan crystals and the absorbance of each well was carried out using a Thermo Scientific Multiskan MK3 ELISA reader (Thermo scientific, Hudson, NH) at 570 nm. Mean and standard deviation for 3 parallel wells for each sample were reported.

To further confirm the cytotoxicity of LAP-Fe_3O_4 NPs, the morphology of HeLa cells treated with LAP-Fe_3O_4 NPs with an Fe concentration ranging from 10 to 100 μg mL^{-1} for 24 h was observed by phase contrast microscopy (Leica DM IL LED inverted phase contrast microscope) with a magnification of 200 × for all samples.

Prussian Blue staining and cellular uptake assay

To confirm the uptake of LAP-Fe_3O_4 NPs, HeLa cells were cultured in a 12-well plate at a density of 2×10^5 cells per well for one day prior to the experiment. Then the cell culture medium was replaced with 1 mL fresh medium containing PBS (control), LAP-Fe_3O_4 NPs at different Fe concentrations (from 0.05 to 0.8 mM) and the cells were incubated for 4 h at 37 °C and 5% CO_2. The cells were then washed with PBS for 3 times, and fixed with 2.5% of glutaraldehyde in PBS for 15 min at 4 °C. After that, the cells were rinsed 3 times with PBS and 1 mL of Perls stain (Perls stain A1/Perls stain A2, *v/v* = 1:1) was added, followed by standing still at 37 °C in the dark for 30 min. Then the cells were washed for 3 times and counterstained with nuclear fast red solution. Finally, the cells were quickly washed 3 times with PBS in 30 s and observed by light microscopy. (Leica DM IL LED inverted phase contrast microscope) with a magnification of 200 × for each sample.

Similar to the protocol described above, HeLa cells were treated with LAP-Fe_3O_4 NPs with an Fe concentration ranging from 0 to 1.2 mM. After 4 h, the cells were washed with PBS for 3 times, trypsinized, resuspended, counted and lysed using an aqua regia solution (nitric acid/hydrochloric acid, *v/v* = 3:1). The cellular uptake of Fe element was measured with ICP-OES.

TEM imaging of HeLa cells

TEM was applied to visually examine the internalization of LAP-Fe_3O_4 NPs in HeLa cells. In brief, HeLa cells were seeded into 10-cm culture dish and cultured at 37 °C and 5% CO_2 overnight to make the cells well adhere on the dish. Then the medium was replaced with fresh medium containing LAP-Fe_3O_4 NPs at an Fe concentration of 0.2 mM and incubated for 4 h at 37 °C and 5% CO_2. After that, the medium was carefully removed and the cells were rinsed with PBS for 3-5 times and fixed at 4 °C using 2.5% of glutaraldehyde PBS solution. After 30 min, the cells were washed for 3 times with PBS, harvested and resuspended in 1 mL PBS. Then the samples were post-processed according to protocols described in the literature.[39] After that, sections with a thickness of 75 nm were obtained using a Reichart Ultramicrotom, and were mounted on copper grids before TEM measurements.

***In vitro* MR imaging of cancer cells**

3×10^6 HeLa cells per well were seeded in a 6-well plate with 2 mL of DMEM at 37 °C and 5% CO_2 for 12 h to bring the cells to confluence. Then the medium was removed and replaced by 2 mL fresh medium containing PBS (control), LAP-Fe_3O_4 NPs at different Fe concentrations ranging from 0.2 mM to 1.6 mM and incubated for 6 h. After that, the cells were washed with PBS for 3-5 times, trypsinized, centrifuged, and resuspended in 1 mL of PBS (containing 0.5% agarose) in 2 mL Eppendorf tubes before MR imaging. The cell T_2-weighted MR imaging was carried out by using a Signa HDxt superconductor clinical MR system (3.0 T, SIEMENS Medical Systems, MAGNETOM VERIO) with 0.9 mm slice thickness, TR = 7500 ms , TE = 77 ms, 9 × 9 cm FOV, and 256 × 320 matrix.

***In vivo* MR imaging of HeLa tumor model**

Animal experiments were approved by the institutional committee, and performed in compliance with the relevant laws and institutional guidelines. To establish the xenografted tumor model, 1.5×10^6 HeLa cells were subcutaneously injected into the left hind leg of BALB/c nude mice (15-20 g, Shanghai Slac Laboratory Animal Center, Shanghai, China). When the tumor volume reached about 350 mm^3 at 3 weeks post-injection, the mice were anesthetized by intraperitoneal injection of pentobarbital sodium (40 mg kg^{-1}), and then the LAP-Fe_3O_4 NPs (930 μg mL^{-1} Fe, in 0.1 mL PBS) were injected into the mice *via* the tail vein. After placing in a custom-built rodent receiver coil (Chenguang Med Tech, Shanghai, China), MR images were obtained before and post-injecton at the time points of 2, 4, and 6 h using a 3.0 T Signa HDxt superconductor clinical MR

system under the same parameters with *in vitro* MR imaging of cancer cells described above.

In vivo biodistribution

To assess the biodistribution of LAP-Fe_3O_4 NPs, the tumor-bearing BALB/c nude mice were anesthetized and injected with LAP-Fe_3O_4 NPs (5 mg mL^{-1} Fe, in 0.1 mL PBS) via tail vein. After 12 h and 24 h, the mice were separately euthanized and the major organs including heart, liver, spleen, lung, kidney and tumor were extracted, weighed and digested by aqua regia for one day, followed by quantification of Fe content by ICP-OES. For comparison, tumor-bearing mice injected with PBS (0.1 mL) were used as control.

In vivo biocompatibility

Two C57 mice (20-25 g, Shanghai Slac Laboratory Animal Center) were used to confirm the long-term organ toxicity of the LAP-Fe_3O_4 NPs. The LAP-Fe_3O_4 NPs (930 μg mL^{-1} Fe, in 0.1 mL PBS) were intravenously injected into one healthy mouse *via* tail vein. After half a month, the mouse was euthanatized. The heart, liver, spleen, lung, and kidney were harvested, and successively fixed with 4% formalin solution, dehydrated, embedded with paraffin, and sectioned. Then the sections were dewaxed, stained with hematoxylin & eosin (H & E) dye and observed by phase contrast microscopy (Leica DM IL LED inverted phase contrast microscope) with a magnification of 200 × for each sample, according to protocols reported in literature.[40] For comparison, these organs from untreated mouse were used as control.

Results and discussion

Synthesis and characterization of LAP-Fe_3O_4 NPs

LAP-Fe_3O_4 NPs were synthesized *via* a controlled coprecipitation route in the presence of LAP (Scheme 1). LAP nanodisks dispersed in water have a high negative surface potential (-34.9 mV) and good colloidal stability. When $FeCl_3$ and $FeCl_2$ are added into LAP solution, Fe^{3+} and Fe^{2+} cations will be attracted close to the surface of LAP nanodisks because of electrostatic interaction. Then Fe_3O_4 NPs form and deposit on LAP nanodisks once pH is increased to trigger the alkaline precipitation. In this way, LAP nanodisks may not only serve as nanoreactors for the formation of Fe_3O_4 NPs, but also simultaneously provide the synthesized LAP-Fe_3O_4 NPs with sufficient colloidal stability. More importantly, the immoblization of Fe_3O_4 onto LAP can separate the Fe_3O_4 NPs apart and significantly suppress the magnetic interparticle interactions thanks to the diamagnetic nature of LAP.[38] This in theory will result in an increase of T_2 relaxivity of LAP-Fe_3O_4 NPs compared to the naked Fe_3O_4 NPs.

After synthesis, LAP-Fe_3O_4 NPs were purified by magnetic separation to remove free laponite in solution. The formation of LAP-Fe_3O_4 NPs was firstly demonstrated by TEM (Fig. 1). Compared to naked Fe_3O_4 NPs with a mean diameter of 8.3 ± 1.6 nm in a clean background (Fig. S1, ESI),

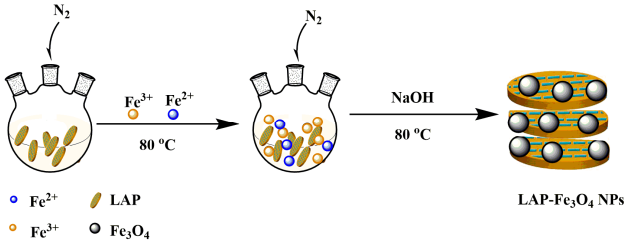

Scheme 1 Schematic illustration of the synthesis of LAP-Fe3O4 NPs.

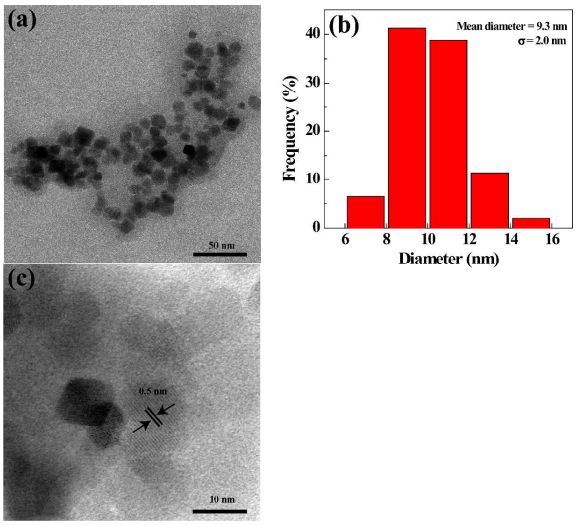

Fig. 1 TEM micrographs and size distribution histograms of LAP-Fe_3O_4 NPs (a, b). (c) The high-magnification TEM image of LAP-Fe_3O_4 NPs.

the formed Fe_3O_4 NPs embedded into LAP displayed a slightly larger mean diameter of 9.3 ± 2.0 nm and were surrounded by some grey shadows, which are the images of LAP with low electron density. It is worth noting that some of Fe_3O_4 NPs in LAP-Fe_3O_4 are octahedral shape, and high-resolution TEM image exhibits that the distance between two adjacent planes is 0.5 nm (Fig. 1c), indicating that the octahedral Fe_3O_4 NPs are enclosed by (111) planes, similar to the magnetic colloidal nanocrystals reported by Mitra, et al..[41] This may be because it is more favorable for Fe_3O_4 NPs to deposit on LAP nanodisks by (111) plane with the lower surface energy, which facilitates the higher growth rate of other planes than that of (111) planes and results in an octahedron shape.[42] To further confirm the component of synthesized NPs, the Mg and Fe element content of LAP-Fe_3O_4 NPs were analyzed by ICP-OES. After magnetic separation and purification, the resultant NPs had both high content of Mg (16.32 μg mL^{-1}) and Fe (59.76 μg mL^{-1}), while pure Fe_3O_4 NPs displayed almost no Mg element and pristine LAP showed only a trace level of Fe (0.49 μg mL^{-1}). Since it is impossible for LAP to move under magnetic field due to its diamagnetic nature, this result indicates that Fe_3O_4 NPs have been successfully immobilized onto LAP, and the formed

LAP-Fe_3O_4 NPs could move as a whole under magnetic field, which is in good agreement with the TEM result.

The crystalline structures of LAP before and after loading Fe_3O_4 NPs were investigated by XRD (Fig. 2a). The XRD pattern of Fe_3O_4 NPs was also set as control. In the XRD pattern of purified LAP-Fe_3O_4 NPs, there are peaks at 2θ of 30.1°, 35.5° and 43.0°, which are the characteristic [220], [311], and [400] planes of Fe_3O_4.[43] The peak position and relative intensity of all diffraction peaks matched well with the standard powder diffraction data of face-centered cubic Fe_3O_4 (JCPDS NO. 65-3107). And in the same time, the peaks of LAP can still be noticed although the intensity decreases as a result of Fe_3O_4 NPs loading.[38] FTIR spectra of LAP, Fe_3O_4 NPs, and LAP-Fe_3O_4 NPs were also collected as shown in Fig. 2b. The FTIR spectra of all samples exhibited a strong band at 3436 cm^{-1} that can be ascribed to the O-H stretching vibrations of H_2O molecules. The peaks at 586-598 cm^{-1} of Fe_3O_4 and LAP-Fe_3O_4 NPs can be assigned to the Fe-O vibration of the magnetite core,[44] and the bands of 1016-1019 cm^{-1} were associated with the Si-O stretching vibration of LAP in LAP and LAP-Fe_3O_4 NPs.[26] Both XRD and FTIR results clearly prove that the synthesized materials are a composite of LAP and Fe_3O_4 NPs.

The mean hydrodynamic diameters and zeta potentials of LAP, Fe_3O_4 NPs, and LAP-Fe_3O_4 NPs were further measured (Table 1). Compared with positively charged Fe_3O_4 NPs, LAP-Fe_3O_4 NPs show a negative zeta potential of -15.9 mV, which is a little higher than that of the original LAP (-34.9 mV). The increase of LAP surface potential may be due to the attachment of positively charged Fe_3O_4 NPs. Moreover, the formation of LAP-Fe_3O_4 can also be demonstrated by the size changes. The mean hydrodynamic size of LAP-Fe_3O_4 NPs increases from 113.1 nm of pristine LAP to 210.2 nm (Fig. S2a, ESI), indicating that Fe_3O_4 NPs (117.8 nm) are immobilized on LAP nanodisks. It is worth mentioning that the hydrodynamic diameter of particles is much higher than that measured by TEM, which is generally ascribed to the fact that DLS measures the size of large clusters of particles in aqueous solution, whereas TEM measures a single nanoparticle in a dry state.[45] For LAP-Fe_3O_4 NPs, because of LAP's non-spherical geometry, the attachment of Fe_3O_4 NPs will drastically change the aspect ratio of the resultant composite and in turn lead to a rather different hydrodynamic sizes. In addition, it is also speculated that embedded Fe_3O_4 NPs may act as bridging spot between two LAP platelets.[38] And the stability of LAP-Fe_3O_4 NPs in water, PBS solution and DMEM culture medium were also investigated as shown in Fig. S2b-d. LAP-Fe_3O_4 NPs exhibited excellent stability in water and their hydrodynamic size has no obvious change in the timespan of 60 days. When dispersed in PBS solution and DMEM culture medium, Fe_3O_4 NPs began to aggregate and precipitate, while LAP-Fe_3O_4 NPs solution kept stable and exhibited negligible differences in DMEM culture medium after 7 days, indicating their good stability in physiological environment. Thus, the approved superior colloidal stability of LAP-Fe_3O_4 NPs is an excellent character for their potential usage in MR imaging contrast enhancement.

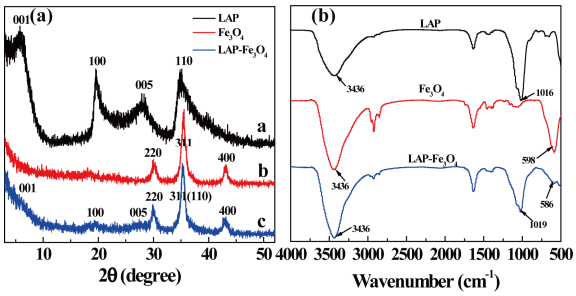

Fig. 2 XRD pattern (a) and FTIR spectroscopy (b) of LAP, Fe_3O_4, and LAP-Fe_3O_4 NPs.

Table 1 Zeta potential and hydrodynamic size of LAP, Fe_3O_4 and LAP-Fe_3O_4 NPs. Data are provided as mean ± SD (n = 3)

Materials	Zeta potential (mV)	Hydrodynamic size (nm)	Polydispersity index (PDI)
LAP	-34.9 ± 1.49	113.1 ± 1.40	0.18 ± 0.01
Fe_3O_4	+20.3 ± 0.71	117.8 ± 3.52	0.26 ± 0.02
LAP-Fe_3O_4	-15.9 ± 2.75	210.2 ± 1.26	0.18 ± 0.01

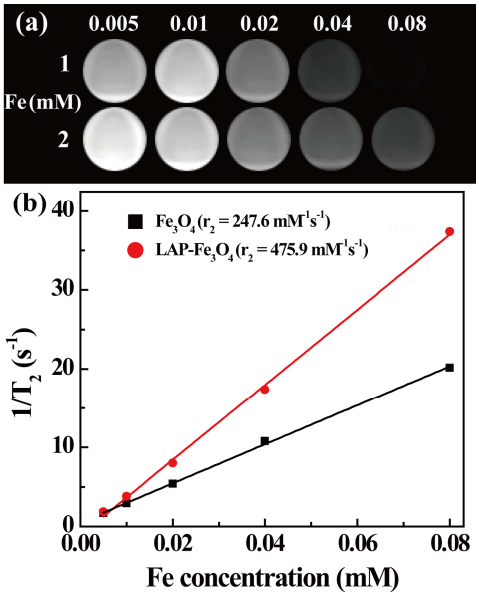

Fig. 3 T_2-weighted MR images (a) and linear fitting of $1/T_2$ (b) of LAP- Fe_3O_4 and Fe_3O_4 NPs at different Fe concentrations (0.005, 0.01, 0.02, 0.04, and 0.08 mM). 1 and 2 represent LAP- Fe_3O_4 and Fe_3O_4 NPs, respectively.

T_2 relaxivity measurements

Fe_3O_4 NPs are commonly used as T_2-weighted MR imaging contrast agent by causing spin-spin relaxation of protons in their vicinity.[8] To explore the MR imaging potential of LAP-Fe_3O_4 NPs, T_2-weighted MR images of LAP-Fe_3O_4 NPs aqueous solution were measured at different Fe concentrations as shown in Figure 3a. Both Fe_3O_4 NPs (control) and LAP-Fe_3O_4 NPs showed a strong T_2-weighted MR imaging contrast effect by generating a 'darkening' contrast in a dose-dependent manner. From the MR images,

it is clear that LAP-Fe_3O_4 NPs cause much lower T_2 signal intensity than Fe_3O_4 NPs at the same Fe concentration. To better compare their imaging ability, transverse relaxivity r_2 of Fe_3O_4 NPs and LAP-Fe_3O_4 NPs were calculated by a linear fitting the inverse T_2 ($1/T_2$) relaxation time *vs* Fe concentrations (Fig. 3b). The r_2 of LAP-Fe_3O_4 NPs (475.9 $mM^{-1}s^{-1}$) is almost two times higher than that of naked Fe_3O_4 NPs (247.6 $mM^{-1}s^{-1}$), which can probably due to two reasons. One is that LAP can separate the Fe_3O_4 NPs apart and suppress the magnetic interparticle interactions due to the diamagnetic nature of LAP, resulting in an increase of T_2 relaxivity of LAP-Fe_3O_4 NPs compared to the naked Fe_3O_4 NPs. The other may be ascribed to formation of octahedral nanocrystals in LAP-Fe_3O_4 NPs, which have a higher saturation magnetization than spherical particles and a corresponding higher relaxivity as well.[42] Considering that the commercial Endorem has an r_2 about 176 $mM^{-1}s^{-1}$, the high r_2 of LAP-Fe_3O_4 NPs does make this type of composite attractive as a potential MR imaging T_2 contrast agent.

Cytotoxicity assay and cell morphology observation

Good cytocompatibility is known to be the very basic prerequisite for the application of any materials in biomedical imaging. Herein, MTT assay is used to evaluate the viability of HeLa cells incubated with LAP-Fe_3O_4 NPs at an Fe concentration up to 100 μg mL^{-1} for 24 h (Fig. 4). It can be clearly seen that the viability of HeLa cells keeps more than 80%, indicating that LAP-Fe_3O_4 NPs shows no appreciable cytotoxicity. Moreover, good biocompatibility of LAP-Fe_3O_4 NPs was further demonstrated by the morphology observation of HeLa cells treated with LAP-Fe_3O_4 NPs (Fig. S3, ESI). Compared with the cells treated with PBS control, HeLa cells treated with LAP-Fe_3O_4 NPs show were attached on the plate and maintained similar normal morphologies, suggesting that cytotoxic effect of LAP-Fe_3O_4 NPs is negligible in the given Fe concentration range.

Cellular uptake assay

As a nano-sized composite material, LAP-Fe_3O_4 NPs will be uptaken by different cells to different extent. The difference in cellular uptake will then translate to different T_2-weighted image darkening effect, which will in turn help distinguish between histologically different cells or tissues. In this study, HeLa cells were used as a model tumor cell line. Prussian blue staining for iron detection, ICP-OES, and cell TEM were employed to investigate the cellular uptake of LAP-Fe_3O_4 NPs. Fig. 5 shows the Prussian blue staining result of HeLa cells incubated with LAP-Fe_3O_4 NPs at different Fe concentrations. In contrast to colorless PBS control, HeLa cells treated with LAP-Fe_3O_4 NPs display increasingly darker blue staining with the increase of NPs concentration, indicating the increased cellular uptake of LAP-Fe_3O_4 NPs. Then the Fe concentrations of HeLa cells treated with LAP-Fe_3O_4 NPs were measured by ICP-OES to quantitatively evaluate the cellular uptake (Fig. S4, ESI). With the increase of LAP-Fe_3O_4 NPs concentration, Fe concentration in HeLa cells gradually increase, which is in line with Prussian blue staining result. Finally, the intracellular localization of the LAP-Fe_3O_4 NPs was visually tracked by TEM (Fig. S5, ESI). After being treated with LAP-Fe_3O_4 NPs for 4 h, HeLa cells can uptake those NPs and LAP-

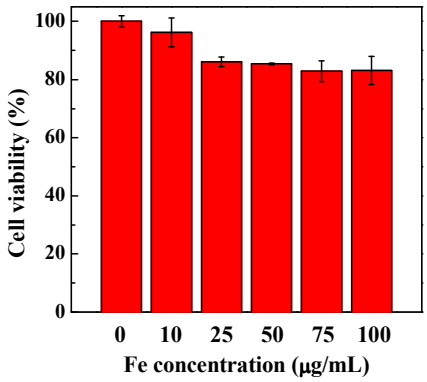

Fig. 4 MTT viability assay of HeLa cells treatment with LAP-Fe3O4 NPs at Fe concentrations of 0-100 μg mL-1 for 24 h. HeLa cells treated with PBS buffer were used as control.

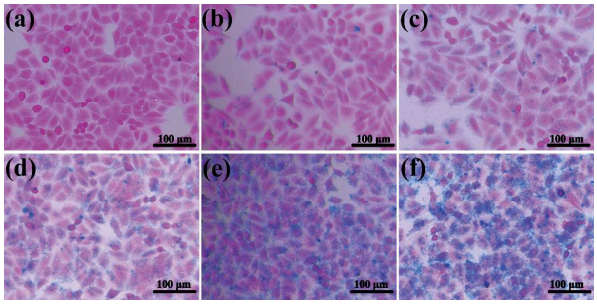

Fig. 5 Prussian Blue staining micrographs of HeLa cells treated with PBS buffer (a), LAP-Fe_3O_4 NPs at Fe concentrations of 0.05 (b), 0.1(c), 0.2 (d), 0.4 (e) and 0.8 (f) mM, respectivily, for 4 h.

Fe_3O_4 NPs were trapped predominantly in the cytoplasm of the cells.

MR imaging of cancer cells *in vitro*

In order to demonstrate the MR imaging performance of LAP-Fe_3O_4 NPs *in vitro*, HeLa cells were incubated with different concentrations of LAP-Fe_3O_4 NPs for 6 h, and then were collected for MR imaging by a 3.0 T Signa HDxt superconductor clinical MR system (Fig. 6). From T_2-weighted MR images in Fig. 6a, it can be clearly seen that MR image of HeLa cells becomes darker with the increase of Fe concentration. Subsequently, the MR imaging signal as a function of Fe concentration is quantitatively analyzed as shown in Fig. 6b. It can be clearly seen the decrease of signal intensity with the increase of LAP-Fe_3O_4 NPs concentration.

***In vivo* MR imaging of HeLa tumor model and major organs**

LAP-Fe_3O_4 NPs (930 μg mL^{-1} Fe, 0.1 mL PBS) were intravenously injected into nude mice bearing HeLa xenograft tumors to further evaluate their capability for *in vivo* MR imaging (Fig. 7a, and color MR images in Fig. S6a, ESI). MR images were acquired before and post 2 h, 4 h and

6 h injection using a 3.0 T Signa HDxt superconductor clinical MR system. To quantify the influence of LAP-Fe_3O_4 NPs on MR imaging, signal-to-noise ratio (SNR) was calculated through the signal intensity of the target area divided by the

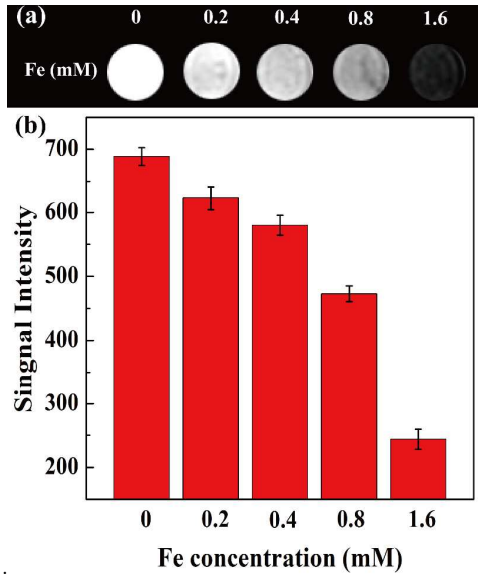

Fig. 6 T_2-weighted MR images (a) and MR signal intensity analysis (b) of HeLa cells after treated with PBS, LAP-Fe_3O_4 NPs at different Fe concentrations for 6 h. 1 and 2 represent the T2-weighted and colored T2-weighted MR images, respectively.

air area's (Fig. 7b). After injection of LAP-Fe_3O_4 NPs, the MR image of liver, kidney and tumor began to darken. It is worth noting that the liver which is abundant of endothelial cells and phagocytic Kupffer cells significantly turns darker owing to the effective uptake of LAP-Fe_3O_4 NPs.[48] Meanwhile, MR signal intensity of tumor reached approximately 50% of loss at 4 h post-injection, and began to recover at 6 h post-injection. This result indicated that some LAP-Fe_3O_4 NPs could diffuse and gradually accumulate in tumor tissue likely by enhanced permeability and retention (EPR) effect, and the metabolism and clearance of LAP-Fe_3O_4 NPs started to show effect in tumor site after 4 h.[46, 47] And the MR signal changes of liver and kidney showed similar profile to that of the tumor, suggesting that LAP-Fe_3O_4 NPs can be captured by liver and metabolized through kidney. Therefore, the synthetic LAP-Fe_3O_4 NPs can exert its higher r_2 relaxivity *in vivo* and may be an effective contrast agent for *in vivo* MR imaging considering its good stability and biocompatibility.

To exclude the decrease trend in T_2-signal simply caused by a result of systemic injection, the tumor-to-muscle signal ratio (TMR) was also calculated to evaluate the relative MR signal intensity of tumor (Fig. S6b, ESI). After the injection of LAP-Fe_3O_4 NPs, about 26~29% of TMR loss could be observed. This result demonstrated that without any targeting ligand, LAP-Fe_3O_4 NPs could passively target and gradually accumulate into tumor and induce the weakening signal of tumor site in the MR image. Taking into consideration of abundant hydroxyl groups on the surface of LAP ready for further modification with various targeting ligands, it is expected that the developed LAP-Fe_3O_4 NPs may be used as a platform for targeted MR imaging of different biological systems, especially for early-stage diagnosis of cancer with high sensitivity and accuracy.

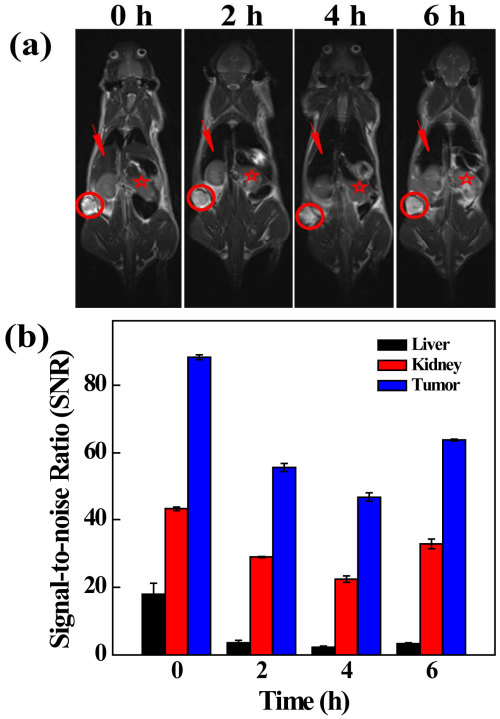

Fig. 7 *In vivo* T_2-weighted images (a) of tumor (red circle), liver (red arrow) and kidney (red star) after intravenous injection of LAP-Fe_3O_4 NPs (930 μg mL^{-1} Fe, in 0.1 mL PBS) for 0 h, 2 h, 4 h, and 6 h. *In vivo* MR signal intensity (b) of liver, kidney and tumor after intravenous injection of LAP-Fe_3O_4 NPs at different time.

In vivo biocompatibility

If used as MR imaging contrast agents, LAP-Fe_3O_4 NPs must be effectively eliminated from the body after the diagnosis and cause no harmful side effects. To trace the fate of those administrated LAP-Fe_3O_4 NPs, Fe contents in several major organs (heart, liver, spleen, lung, kidney, and tumor) of mice after intravenous injection for 0 h, 12 h and 24 h were measured by ICP-OES (Fig. S7, ESI). After 12 h, the Fe concentrations in heart, kidney and tumor are similar to those before injection, indicating that LAP-Fe_3O_4 NPs have been eliminated from those organs. After 24 h, Fe concentrations in liver, spleen and lung decreased, suggesting that LAP-Fe_3O_4 NPs accumulated in body can be metabolized and cleared out of body in a reasonable time frame of 24 h post-injection.

To confirm the long-term organ toxicity of LAP-Fe_3O_4 NPs *in vivo*, the heart, liver, spleen, lung, and kidney of healthy mouse intravenously injected with LAP-Fe_3O_4 NPs (930 μg mL^{-1} Fe, in 0.1 mL PBS) were examined at half a month post-injection. The major organs were harvested, processed, sectioned, and H & E stained prior to examinations. As clearly shown in Fig. 8, the morphologies of cells in the studied organ sections have no significant change when

compared to the control mouse without treatment. These results suggest that the LAP-Fe_3O_4 NPs do not display any apparent toxicity to the organs, which is critical for their further *in vivo* biomedical application.

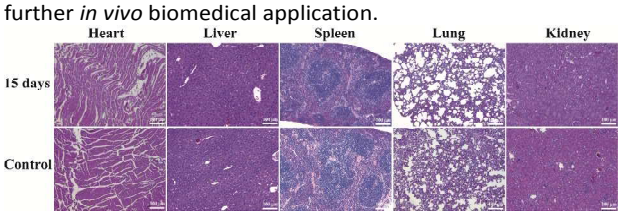

Fig. 8 H & E staining section images of heart, liver, spleen, lung and kidney in healthy nude mouse at 15 day post intravenous injection of LAP-Fe_3O_4 NPs (930 μg mL^{-1} Fe, in 0.1 mL PBS). Organs from the untreated mice were used as control.

Conclusions

In summary, a facile approach to the synthesis of LAP-Fe_3O_4 NPs *via* immobilization of Fe_3O_4 on LAP has been developed. The obtained LAP-Fe_3O_4 NPs possess several important advantages including water-dispersibility, good colloidal stability, and cytocompatibility. Importantly, the r_2 of LAP-Fe_3O_4 NPs is about twice higher than that of naked Fe_3O_4 NPs. Both i*n vitro* tumor cell MR imaging and *in vivo* tumor grafted nude mice MR imaging showed obvious signal intensity change in the presence and with the administration of LAP-Fe_3O_4 NPs respectively owing to the cellular uptake of those NPs, which demonstrates the promise of using LAP-Fe_3O_4 NPs as T_2-weighted contrast agent for MR imaging. Moreover, taking into consideration of the unique layered structure and characteristics, LAP can be further loaded with various anti-cancer drugs (e.g., DOX), or modified with certain homing moieties for active targeting. Therefore, the LAP-Fe_3O_4 NPs system has the potential to be used as a versatile theranostic platform to construct more complex and powerful nanosized diagnostic/therapeutic materials.

Acknowledgements

The authors thank Prof. Kai Sun from Michigan University and Prof. Wei Liu from University of Electronic Science and Technology of China for the helpful discussions and instrumental support in TEM analysis. We acknowledge financial support of this work from the National Natural Science Foundation of China (81201189, 81401458, 31400816, and 21273032), the Fund of the Science and Technology Commission of Shanghai Municipality (12nm0501900 and 14ZR1432400), and the Science and Technology Collaboration Fund between China and Hungary, Ministry of Science and Technology.

Notes and references

1. J. Li, Y. He, W. Sun, Y. Luo, H. Cai, Y. Pan, M. Shen, J. Xia and X. Shi, *Biomaterials*, 2014, **35**, 3666-3677.
2. Y. Hu, J. Li, J. Yang, P. Wei, Y. Luo, L. Ding, W. Sun, G. Zhang, X. Shi and M. Shen, *Biomater. Sci.* , 2015, **3**, 721-732.
3. J. Fang, P. Chandrasekharan, X.-L. Liu, Y. Yang, Y.-B. Lv, C.-T. Yang and J. Ding, *Biomaterials*, 2014, **35**, 1636-1642.
4. Y. Ding, S.-X. Rao, T. Meng, C. Chen, R. Li and M.-S. Zeng, *Eur. J. Radiol.*, 2014, **24**, 959-966.
5. L. Wang, H. Zhang, Z. Zhou, B. Kong, L. An, J. Wei, H. Yang, J. Zhao and S. Yang, *J. Mater. Chem. B* 2015, **3**, 1433-1438.
6. H. Yang, C. Qin, C. Yu, Y. Lu, H. Zhang, F. Xue, D. Wu, Z. Zhou and S. Yang, *Adv. Funct. Mater*, 2014, **24**, 1738-1747.
7. G. Wang, S. Inturi, N. J. Serkova, S. Merkulov, K. McCrae, S. E. Russek, N. K. Banda and D. Simberg, *ACS Nano*, 2014, **8**, 12437-12449.
8. X. Shi, T. P. Thomas, L. A. Myc, A. Kotlyar and J. R. Baker, Jr., *Phys. Chem. Chem. Phys.* , 2007, **9**, 5712-5720.
9. Y. Hu, J. Li, M. Shen and X. Shi, *Chin. Phys. B*, 2014, **23**, 78704-78711.
10. H. Cai, X. An, J. Cui, J. Li, S. Wen, K. Li, M. Shen, L. Zheng, G. Zhang and X. Shi, *ACS Appl. Mater. Interfaces*, 2013, **5**, 1722-1731.
11. J. Li, L. Zheng, H. Cai, W. Sun, M. Shen, G. Zhang and X. Shi, *Biomaterials*, 2013, **34**, 8382-8392.
12. M. Shen and X. Shi, *Nanoscale*, 2010, **2**, 1596-1610.
13. S. Langereis, A. Dirksen, T. M. Hackeng, M. H. P. van Genderen and E. W. Meijer, *New J. Chem.*, 2007, **31**, 1152-1160.
14. B. Pan, D. Cui, Y. Sheng, C. Ozkan, F. Gao, R. He, Q. Li, P. Xu and T. Huang, *Cancer Res.*, 2007, **67**, 8156-8163.
15. X. Shi, S. H. Wang, S. D. Swanson, S. Ge, Z. Cao, M. E. Van Antwerp, K. J. Landmark and J. R. Baker, Jr., *Adv. Mater.* , 2008, **20**, 1671-1678.
16. Y. Xu, Y. Qin, S. Palchoudhury and Y. Bao, *Langmuir*, 2011, **27**, 8990-8997.
17. Y. Xu, S. Palchoudhury, Y. Qin, T. Macher and Y. Bao, *Langmuir*, 2012, **28**, 8767-8772.
18. X. Sun, F. Liu, L. Sun, Q. Wang and Y. Ding, *J. Inorg. Organomet. Polym. Mater.*, 2012, **22**, 311-315.
19. H. Cai, K. Li, M. Shen, S. Wen, Y. Luo, C. Peng, G. Zhang and X. Shi, *J. Mater. Chem.*, 2012, **22**, 15110-15120.
20. H. H. Yiu, M. R. Pickard, C. I. Olariu, S. R. Williams, D. M. Chari and M. J. Rosseinsky, *Pharm Res*, 2012, **29**, 1328-1343.
21. S. L. Tawari, D. L. Koch and C. Cohen, *J. Colloid Interface Sci.* , 2001, **240**, 54-66.
22. B. Ruzicka and E. Zaccarelli, *Soft Matter*, 2011, **7**, 1268-1286.
23. M. Elzbieciak, D. Wodka, S. Zapotoczny, P. Nowak and P. Warszynski, *Langmuir*, 2009, **26**, 277-283.
24. G. Cavallaro, G. Lazzara, S. Milioto and F. Parisi, *J Therm Anal Calorim*, 2014, **117**, 1293-1298.
25. M. M. Lezhnina, T. Grewe, H. Stoehr and U. Kynast, *Angew. Chem., Int. Ed.*, 2012, **51**, 10652-10655.
26. S. Wang, Y. Wu, R. Guo, Y. Huang, S. Wen, M. Shen, J. Wang and X. Shi, *Langmuir*, 2013, **29**, 5030-5036.
27. K. Li, S. Wang, S. Wen, Y. Tang, J. Li, X. Shi and Q. Zhao, *ACS Appl. Mater. Interfaces* 2014, **6**, 12328-12334.
28. G. Wang, D. Maciel, Y. Wu, J. Rodrigues, X. Shi, Y. Yuan, C. Liu, H. Tomas and Y. Li, *ACS Appl. Mater. Interfaces* 2014, **6**, 16687-16695.
29. Y. Wu, R. Guo, S. Wen, M. Shen, M. Zhu, J. Wang and X.

Shi, *J. Mater. Chem. B* 2014, **2**, 7410-7418.
30. G. Chen, D. Li, J. Li, X. Cao, J. Wang, X. Shi and R. Guo, *New J.Chem.*, 2015, **39**, 2847-2855.
31. J. V. de Melo, S. Cosnier, C. Mousty, C. Martelet and N. Jaffrezic-Renault, *Anal. Chem.*, 2002, **74**, 4037-4043.
32. C. Mousty, *Anal. Bioanal. Chem.* , 2010, **396**, 315-325.
33. N. Aihara, K. Torigoe and K. Esumi, *Langmuir*, 1998, **14**, 4945-4949.
34. Y. Lambert, R. Le Dantec, Y. Mugnier, C. Galez, J.-C. Plenet, J. Bouillot, H. Hayakawa and Y. Uesu, *Jpn. J. Appl. Phys.*, 2006, **45**, 7525-7530.
35. T. Szabó, A. Bakandritsos, V. Tzitzios, S. Papp, L. Korösi, G. Galbács, K. Musabekov, D. Bolatova, D. Petridis and I. Dékány, *Nanotechnology*, 2007, **18**, 285602.
36. J.-L. Besombes, S. Cosnier, P. Labbe and G. Reverdy, *Anal. Chim. Acta*, 1995, **317**, 275-280.
37. J.-L. Besombes, S. Cosnier and P. Labbe, *Talanta*, 1997, **44**, 2209-2215.
38. V. Tzitzios, G. Basina, A. Bakandritsos, C. G. Hadjipanayis, H. Mao, D. Niarchos, G. C. Hadjipanayis, J. Tucek and R. Zboril, *J. Mater. Chem.* , 2010, **20**, 5418-5428.
39. S. H. Wang, X. Shi, M. Van Antwerp, Z. Cao, S. D. Swanson, X. Bi and J. R. Baker, *Adv. Funct. Mater*, 2007, **17**, 3043-3050.
40. C. Peng, J. Qin, B. Zhou, Q. Chen, M. Shen, M. Zhu, X. Lu and X. Shi, *Polym. Chem.* , 2013, **4**, 4412-4424.
41. A. Mitra, J. Mohapatra, S. S. Meena, C. V. Tomy and M. Aslam, *J. Phys. Chem. C,*, 2014, **118**, 19356-19362.
42. Z. Wang, *J. Phys. Chem. B* 2000, **104**, 1153-1175.
43. J. Li, L. Zheng, H. Cai, W. Sun, M. Shen, G. Zhang and X. Shi, *ACS Appl. Mater. Interfaces*, 2013, **5**, 10357-10366.
44. J. Hong, D. Xu, J. Yu, P. Gong, H. Ma and S. Yao, *Nanotechnology*, 2007, **18**, 6 pp.-6 pp.
45. H. Liu, Y. H. Xu, S. H. Wen, Q. Chen, L. F. Zheng, M. W. Shen, J. L. Zhao, G. X. Zhang and X. Y. Shi, *Chem. Eur. J.*, 2013, **19**, 6409-6416.
46. L. Bu, J. Xie, K. Chen, J. Huang, Z. P. Aguilar, A. Wang, K. W. Sun, M.-S. Chua, S. So, Z. Cheng, H. S. Eden, B. Shen and X. Chen, *Contrast Media Mol. Imaging*, 2012, **7**, 363-372.
47. V. Torchilin, *Adv. Drug Delivery Rev.*, 2011, **63**, 131-135.
48. H. Li, K. Yan, Y. Shang, L. Shrestha, R. Liao, F. Liu, P. Li, H. Xu, Z. Xu and P. K. Chu, *Acta Biomater.*, 2015, **15**, 117-126.
49. Y.-X. J. Wang, *Quant Imaging Med Surg*, 2011, **1**, 35-40.

Graphical Abstract

Laponite-stabilized iron oxide nanoparticles for *in vivo* MR imaging of tumors

Ling Ding,[a§] Yong Hu,[a§] Yu Luo,[a] Jianzhi Zhu,[a] Yilun Wu,[a] Zhibo Yu,[a] Xueyan Cao,[a] Chen Peng,*[b] Xiangyang Shi,*[ac] Rui Guo*[a]

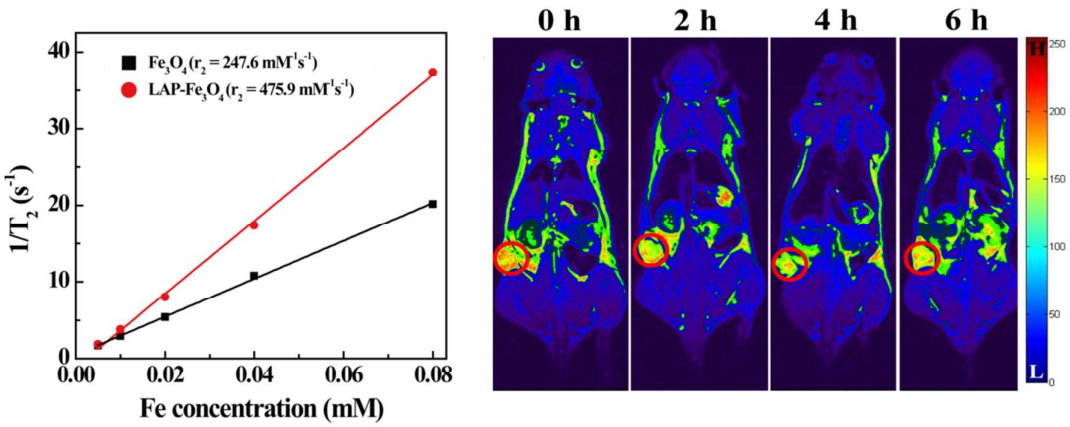

Laponite-stabilized iron oxide nanoparticles with great colloidal stability and exceptionally high T_2 relaxivity are synthesized by a facile controlled coprecipitation method, and can significantly enhance the contrast of a xenografted tumor model, indicating their tremendous potential in MR imaging applications.